GIS-based solar radiation modelling for photovoltaic potential in cities: A sensitivity analysis for the evaluation of output variability range

Energy Reports 12 (2024) 4656–4669

Contents lists available at ScienceDirect

Energy Reports

journal homepage: www.elsevier.com/locate/egyr

GIS-based solar radiation modelling for photovoltaic potential in cities: A sensitivity analysis for the evaluation of output variability range

Sebastiano Anselmo [a], Ali Safaeianpour [a], Sara Torabi Moghadam [a], Maria Ferrara [b,*]

[a] Interuniversity Department of Regional and Urban Studies and Planning, Politecnico di Torino, Italy
[b] Department of Energy, Politecnico di Torino, Italy

ARTICLE INFO

Keywords:
Urban energy planning
Solar energy
Energy simulation
Digital twin
ArcGIS
QGIS

ABSTRACT

Currently, there is increasing attention to matching the buildings' energy demand with energy produced by renewable sources. This approach serves to both reduce the environmental footprint, the target of several European policies and initiatives and ensure access to energy for everyone worldwide, aligning with one of the aims of the United Nations Agenda 2030. Urban environments are suitable for the installation of photovoltaic panels, which can be easily integrated within roofs to minimise land use and installation costs. Multiple studies focused on solar radiation as the most critical element affecting the estimation of the photovoltaic potential, in particular by resorting to Geographic Information Systems (GIS). Among different tools, which are useful for integrating layers with different spatial resolutions, the r.sun function embedded in GRASS GIS has been selected as the most suitable to capture complex variations resulting from weather and geographical parameters. However, a gap in the literature has emerged as no study is available to define the precision degree of the tool when inputting parameters derived from various data sources based on different model assumptions. The scope of this research is to collect open-access weather inputs and quantify the solar radiation output along with its variability range. Based on 28 test plans, resulting from the combination of input parameters from alternative data sources, this research quantified the output variability range to be ±20 %, thus requiring additional processing to increase the precision. The paper concludes with a critical assessment of the strengths and weaknesses of the current research, emphasizing the importance of validating the results with measured values in forthcoming research, to move from precision to accuracy evaluation.

1. Introduction

Climate change is a threat which affects not only the environment but also human activities. The energy sector has been identified as one of the principal targets to reduce effectively carbon emissions, thus mitigating the effects of climate change. In particular, 70 % of energy-related emissions derive from urban contexts, where – according to the International Energy Agency (IEA, 2016) – it is possible to cut them by two-thirds effectively.

European policymakers are addressing this issue in a twofold way: on the one hand, there is increasing attention towards the improvement of the energy performance of the building stock, on the other hand, the remaining energy demand is to be met through Renewable Energy Sources (RESs). This approach is the core of the Energy Performance of Buildings Directive recast (European Parliament and Council, 2024). However, the principal reference to clean energy production is the Renewable Energy Directive, first issued in 2009 (European Parliament and Council, 2009), whose recast (European Parliament and Council, 2018) promotes the creation of Renewable Energy Communities – non-commercial cooperations of prosumers – and supporting frameworks at various administrative levels. Among the RESs – in particular in urban environments – specific attention is given to photovoltaic (PV) technologies because of the possibility of minimising land take while maximising the proximity between production and consumption locations. Indeed, while solar farms require extensive areas and dedicated infrastructure, PV panels can be integrated within roofs, causing as only impacts the emissions related to their installation and the increased reflectance – potentially leading to urban canyon phenomena. The relevance of solar energy is further testified by the role it has in the principal initiatives launched by the European Commission following the energy crises derived from recent geopolitical issues and challenges posed by the COVID-19 pandemic. The REPowerEU Plan (European

* Corresponding author.
E-mail address: maria.ferrara@polito.it (M. Ferrara).

https://doi.org/10.1016/j.egyr.2024.10.031
Received 28 June 2024; Received in revised form 30 September 2024; Accepted 18 October 2024
Available online 30 October 2024

Commission, 2022a) – launched in 2022 to modify the energy mix in order to make Europe self-produce most of its energy demand – includes the solar energy strategy (European Commission, 2022b), targeting the installation of 600 GW of PV production by 2030 and setting an intermediate milestone in 2023, with the installation of 320 GW. This ambitious goal is structured in three main initiatives: i) the European Solar Rooftops Initiative aims at exploiting roofs as available surfaces to produce clean energy; ii) a large-scale skills partnership was launched in March 2023 to train skilled workforce in the renewable energy sector; iii) the solar PV Industry Alliance ensures investment opportunities and value retain in Europe, diversifying the supply chain to reduce European dependency from foreign manufacturers. A change in the energy mix is required also by Target 7.2 of the Agenda 2030 (United Nations General Assembly, 2015), aiming to "increase substantially the share of renewable energy in the global energy mix" as part of the global target to ensure access to energy for all (Sustainable Development Goal 7).

1.1. Background

In this context, there is an increasing need for supporting tools enabling the extraction of the most productive sites – on a large scale – and pitches – at urban or district scale.

In the energy sector, Geographic Information Systems (GIS) have recently emerged as powerful tools for extensive modelling, adequately meeting the need to consider simultaneously multiple informative layers (Yu et al., 2021). As the estimation of the photovoltaic potential is a complex task, which needs to take into account several parameters – related to roof geometry, characteristics of the surrounding objects, and weather – with different spatial and temporal resolutions, multiple scholars have resorted to GIS to carry out solar-related analyses. Recently, specific attention has been given to three-dimensional applications in the GIS domain, making it possible to model complex roof geometries and cast shadows without simplifying the urban morphology.

A review by Anselmo and Ferrara (Anselmo and Ferrara, 2023) has explored the principal 3D GIS-based techniques for PV potential estimation by critically analysing 125 research papers worldwide. It emerged that the interest towards photovoltaics has constantly increased, as testified by the number of publications in scientific journals. Approximately 50 % of studies have been carried out in Europe, with another 32 % from Asia: the countries with the most publications are Italy and China. The scale of analysis is very different, from regional cities – e.g., Hong Kong in the research by Peng et al. (2016) – to public transport stops (Fijałkowska et al., 2022; Ren et al., 2022).

Out of the considered studies, 42 % focus on solar radiation. Indeed, solar radiation is one of the principal elements of interest when studying photovoltaic potential, as it is the only parameter which cannot be calculated in laboratories but rather needs site-specific modelling.

In order to include the third dimension in solar radiation calculation, most studies used a 3D model or a Digital Surface Model (DSM), with some of them(Bremer et al., 2016; Fijałkowska et al., 2022; Lindberg et al., 2015; Redweik et al., 2012) making a combined use of both. While some scholars developed new tools for calculating solar radiation, such as Solar3D (Liang et al., 2020) and DeepRadiation (Nakhaee and Paydar, 2023), there is nearly half of the authors took advantage of tools embedded in the two most diffused GIS software – Area Solar Radiation in ArcGIS Pro and r.sun.insoltime in QGIS –, both based on DSMs. As the description of the two tools is out of the scope of the paper, please refer to Freitas et al. (Freitas et al., 2015) and Anselmo & Ferrara (Anselmo and Ferrara, 2023) for an extensive explanation of the two tools. While the r.sun module can work in two modes – for a specific time or aggregated on a daily basis – there is a prevalence of the latter, as in (Eldesoky et al., 2019; Fichera et al., 2018; Hubinský et al., 2023; Liang et al., 2014). As for the input, different studies resort to different databases, local – e.g., the ARPA Dataset in Piedmont Region, Italy (Mutani et al., 2019) – or global – such as the NASA database used by Soares et al. (2020) –, while there are no studies where different inputs have been considered in the same research. From this, it derives a general impossibility to define a precision range of the used tools.

1.2. Scope, novelty and structure of the work

Recognising the mentioned need for tools and methodologies supporting technicians and policymakers in understanding the photovoltaic potential of their areas of interest, with specific attention to the precision and accuracy of the tools themselves, it is necessary to define the reliability of both inputs and outputs of solar radiation estimation models. Therefore, this study aims to calculate solar radiation and provide a variability range based on open data and open software, thus focusing on QGIS. The research is divided into two principal sections. The first consists of the research on the required inputs and consequent data gathering from open sources, while the second is the actual calculation. This comprehensive analysis aims to fill a gap in the precision of GIS-based solar estimation, focusing on PV resource potential, as defined by Bódis et al. (2019) While different studies have validated the accuracy of their results against online tools – such as Agugiaro et al. (2013) with PVGIS –, observed data (Lohani et al., 2018; Singh et al., 2020; Yoon et al., 2020) or other software (Desthieux et al., 2018; Esclapés et al., 2014; Liang and Gong, 2017), the novelty of this study lays in the assessment of the variability based on alternative inputs, all gathered from authoritative data sources. Based on the results of this research, it could be possible to define the reliability of the outcomes even without validation data –costly to acquire in terms of both time and money due to the need to create an adequate time series.

The presented methodology is applied to a case study located in the City of Turin, one of the 100 cities participating in the European Mission Climate Neutral and Smart Cities (European Commission, 2023). In particular, the Area of Interest is a district in the northern part of the City which is currently an exemplary pilot site for intensive research activities in the field (Anselmo et al., 2023).

Given the strategic nature of the PV potential, it is crucial to use this analysis as one of the principal layers for Urban Digital Twins, virtual replicas of a city as a complex system which enables simulations on the object alone or as part of its environment (Minerva et al., 2020). In compliance with the Renewable Energy Directive, this thematic layer of the Urban Digital Twin could support the realisation of Renewable Energy Communities by highlighting the most productive areas where to locate PV panels, taking into account multiple inputs and alternative scenarios to evaluate the most suitable solution.

Section 2 introduces the methodological aspects related to this research – divided into data gathering and estimation of the solar radiation –, and the case study. Results are presented in the following section and discussed in Chapter 4, which compares alternative calculations to answer the original research question. Conclusions and future perspectives are included in Section 5.

2. Methodology

As mentioned in the introduction, this paper aims to provide a variability range in solar radiation estimation by resorting to open data and software. Therefore, the methodology can be seen as divided into a preparatory phase of data gathering and the actual elaboration in QGIS software. In particular – as shown in Fig. 1– the process starts with the identification of the parameters required by the solar radiation modelling tool. Second, necessary data are gathered from different sources and aggregated in 28 test plans and 3 input configurations (monthly, seasonal and yearly) before the actual calculation of solar radiation. Results are referred to four representative buildings to explore the principal trends across the 84 elaborations.

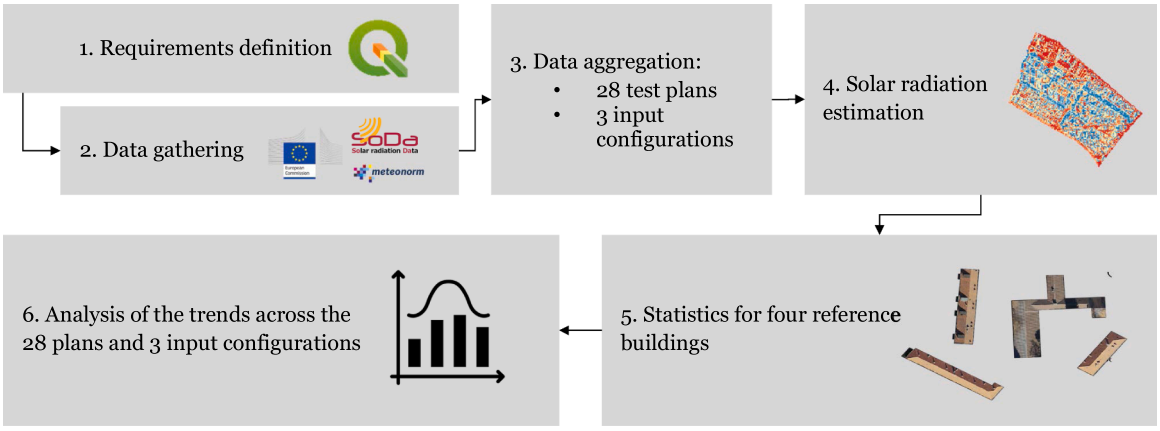

Fig. 1. Schematical representation of the proposed methodology.

2.1. Selected tool

Based on the state-of-the-art in solar radiation modelling and photovoltaic potential estimation, it appears that Area Solar Radiation (embedded in ArcGIS Pro) and r.sun (integrated in QGIS) are the two most diffused GIS-based tools for the calculation of solar radiation. In this study, it was chosen to focus on QGIS to allow better dissemination of the results, removing technological barriers given by the licensing requirements of ArcGIS Pro. Moreover, most of the inputs are open-source, thus making it coherent to use open software.

The r.sun module, developed by Jaroslav Hofierka and Marcel Suri in 2007 (Hofierka et al., 2024), is part of GRASS (Geographic Resources Analysis Support System) GIS, now integrated within QGIS software. The r.sun.insoltime tool computes solar radiation as global or divided into its three principal components (direct, diffuse, reflected) based on 2.5D information on elevation, slope and orientation. Solar radiation is estimated on a daily basis – differently from Area Solar Radiation (ASR) which allows monthly and yearly calculations too – by estimating solar geometry from previous research. It is a clear sky model, not able to take into account spatial and temporal variations of clouds.

The r.sun module – whose computation formulas were presented at the GRASS user conference (Hofierka and Suri, 2002) – does not have any limitations in terms of spatial extent and resolution besides the ones deriving from the performance of the used device (Hofierka et al., 2024). Because of the possibility of running the model on large areas, most parameters are inputted as raster files, making it possible to return spatial variations. On the contrary, ArcGIS Pro ASR gives the user the possibility to input only single numerical values.

All the results are provided in the form of raster files, with spatial resolution deriving from the raster inputs. Solar radiation outputs – quantifying global, beam, diffuse and reflected radiation – are provided in $Wh/m^2/day$, while insolation time is quantified in hours.

2.2. Data collection

The data collection phase consists of the creation of a reliable dataset to be used as input for the solar radiation estimation. Both geometrical and weather information are crucial for accurate simulations, thus requiring a sound set of inputs.

2.2.1. Required inputs

The first inputs of r.sun.insoltime are related to the geometric characteristics. The first raster to be selected is the elevation layer, returning height information in metres. Successively, orientation and slope are required. This makes it possible for r.sun not to compute geometrical parameters at each iteration – differently from ASR –, thus reducing the elaboration time. In case solar radiation is to be calculated for a single geometry, it is possible to input a single value for both.

The only other mandatory parameter is the day of the year, where 1st January is day 1 and 31st December is day 365 (Hofierka et al., 2024). As previously mentioned, it is not possible to carry out simulations on multiple days.

Weather parameters – optional – are all provided as raster files except for the albedo coefficient, for which the possibility of providing a single value is given.

The Linke turbidity factor – one of the principal parameters to correct the biases deriving from the clear sky estimation – characterises the real atmosphere by quantifying the number of clean dry atmospheres necessary to have the same radiation attenuation effect (Eltbaakh et al., 2012). Therefore, it is effective in assessing the effect of aerosols (Eltbaakh et al., 2012) and water vapours (Remund et al., 2003). It depends on air mass, the irradiance on a surface normal to the solar beam, the solar constant and the reduction factor for mean solar distance at a specific moment (Page, 1981). It is crucial in assessing both the beam irradiance normal to the solar beam B_{0c} – from which the beam irradiance on horizontal and inclined surfaces are calculated – and the diffuse component on horizontal surface D_{hc}, as shown in Eqs. 1 and 2:

$$B_{0C} = G_0{}^{-0.662 T_{LK} m \delta_R(m)} \tag{1}$$

$$D_{hc} = G_0 T_n(T_{LK}) F_d(h_0) \tag{2}$$

Where:

- G_0 is the extraterrestrial irradiance
- T_{LK} is the Linke turbidity factor
- m is the relative optical air mass
- δ_R is the Rayleigh optical thickness at air mass m
- T_n is a diffuse transmission function dependent on the Linke turbidity factor
- F_d is a diffuse solar altitude function dependent on the solar altitude h_0.

Albedo quantifies the reflectance of urban surfaces. It is the percentage of reflected sunlight, which affects temperature, evaporation and heat transfer (Coakley, 2003). It is instrumental for the calculation of the clear-sky diffuse ground reflected irradiance on an inclined surface R_i (Eq. 3):

$$R_i = \rho_g G_{hc} r_g(\gamma_N) \tag{3}$$

Where:

- ρ_g is the mean ground albedo
- G_{hc} is the global horizontal irradiance
- $r_g(\gamma_N)$ is a fraction of the ground viewed by an inclined surface.

In this study it is considered as negligible, in order to quantify only radiation coming directly from the sky: it is manually set to be zero.

Beam and diffuse coefficients, together with the Linke turbidity factor, are the main parameters to correct biases deriving from the clear sky model. Given the assumption of reflected energy to be negligible, their sum is equal to 1, as the total solar radiation is defined as the sum of direct, diffuse and reflected components. Diffuse radiation is generated by atmospheric scattering, with micro-reflections caused by suspended particles – such as water vapours and pollutants – whose impact is particularly evident in urban areas.

Advanced parameters are kept by default. They calibrate the model in terms of time step to calculate daily radiation – one every 0.5 hours – and the sampling distance coefficient – 1.

In order to speed up the calculation, based on the decision to focus on global radiation alone, the only output which is calculated is the global radiation, skipping the production of other outputs.

2.2.2. Data sources

Based on the findings of the above-mentioned recent review on the current trends for the calculation of PV potential (Anselmo and Ferrara, 2023), most studies which resort to existing databases to gather weather parameters take advantage of the Photovoltaic Geographical Information System (PVGIS) (European Commission, 2022c) by the Joint Research Center of the European Commission, Solar radiation Data (SoDA) (Solar Energy Services for Professionals, 2022) and Meteonorm software (Meteotest, 2024).

PVGIS is a web GIS providing information on solar radiation and theoretical PV production worldwide. The most recent database is SARAH-2.1, with data from 2005 to 2020, but SARAH and ERA5 databases – including information from 2005 to 2016 and from 2005 to 2020 respectively – can be exploited too. Radiation data can be accessed with different temporal resolutions, from hourly to monthly. In the case of daily or monthly data, it is also possible to visualise results on graphs. It is also possible to download the Typical Meteorological Year, in epw or csv format. PVGIS takes into account shadows only from a Digital Terrain Model, not considering any natural or anthropic element apart from the natural morphology when casting shadows, on a 1 km x 1 km grid.

SoDa, based on the HelioClim-3 solar radiation database and Meteosat-11 satellite, provides services related to solar energy, meteorological, weather, altitude and astronomic data. Its information ranges from February 2004 to the access date, with different time steps available – from 1 minute to 1 month.

Meteonorm software generates Typical Meteorological Years based on long-term monthly averages for global locations. In this research, the "contemporary dataset", covering radiation data from 2001 to 2020, was used (Remund et al., 2023). Meteonorm values derive from satellite acquisitions, ground measurements – with and without the direct measurement of solar radiation – and interpolated values from Aeronet stations. The closest Aeronet station is more than 100 km away, in Ispra (VA), while weather stations are located at Turin Airport (Caselle Torinese, TO) and at the top of the highest elevation of Turin Hill – Maddalena Hill (715 masl).

Additional data about the Linke Turbidity Factor are available in the literature – specifically for Turin (Fracastoro et al., 2011), where the Area of Interest is located – and as default values of the r.sun module (Hofierka et al., 2024).

As for the Digital Elevation Model, it was chosen to resort to the highest available geodata, made available for this study by the SDG11 Lab (Politecnico di Torino, 2024). An alternative is provided by the Piedmont Region Geoportal (Regione Piemonte, 2024), where a DSM is provided with a 5 m x 5 m resolution.

2.3. Solar radiation estimation

The core of the study is the actual estimation of solar radiation based on the input dataset realised in the preliminary phase. Based on the numerosity of the available sources, plans for the tests are to be drafted to verify all possible combinations of the gathered values.

Since the r.sun.insoltime tool computes solar radiation on a daily basis, it is necessary to define a significant day for each month – extracted from (Klein, 1977) – and note the number of days of each month in order to compute the monthly cumulative solar radiation. The adopted values are plotted in Table 1.

Based on the need to input raster files in the r.sun.insoltime tool, data preparation includes the creation of one raster file for each month, for both the Linke turbidity factor and diffuse coefficient – or diffuse-to-global radiation ratio (DG ratio). Subsequently, one iteration has to be carried out for every month. The output is to be further processed by multiplying the values of each cell by the number of days for that month, thus obtaining the monthly global radiation.

This process is very time-consuming and inefficient, because of the need to launch a new processing every time the output has been generated. Moreover, several temporary files to be later deleted are produced. However, it is possible to resort to the QGIS Graphic Modeler. This tool allows us to realise a composite function starting from QGIS tools, graphically visualising the process. A new function with some inputs given by the user and some others set by default is realised, launching the processes subsequently without the need to manually run them. Moreover, only the necessary outputs are stored in the computer memory, while intermediate files are removed from the cache.

A first added value of the Graphic Modeler is the possibility of not computing – and storing – slope and orientation, which are automatically elaborated at the beginning of the process. Moreover, instead of producing a raster file for Linke turbidity factor and DG ratio, it is possible to input numerical values and automatically produce the rasters. Indeed, in this case, a small urban portion is considered, thus making it sufficient to use a single value for weather parameters. In the most complex case, where weather parameters are inputted with monthly time step, the user needs to manually input 24 values – 12 for Linke turbidity factor and 12 for DG ratio. Therefore, a trial on possible simplifications is provided, aggregating these two inputs seasonally and yearly. In the first case, the number of inputs is reduced to 6:

- 2 for winter, encompassing January, February, November and December;
- 2 for spring and autumn, encompassing March, April, September and October;
- 2 for summer, encompassing the months from June to August.

In the second time configuration, a single Linke turbidity factor and DG ratio values are provided.

2.4. Case study

The study area falls within the *Barriera di Milano* district, in the Northern part of the City of Turin, Italy. It is a densely populated urban area, characterised by heterogeneous land uses and social marginality. It is the interest of the City to work on this area to create Renewable Energy Communities in order to fight energy poverty, push the redevelopment of the neighbourhood and fully exploit all available surfaces – with special attention to commercial and industrial buildings, generally wider and flatter compared to residential ones. In order to have the possibility to validate the results in the future by installing photovoltaic panels or weather stations on the pitches, a cluster including publicly-owned buildings was identified. As shown in Fig. 2 it is located between two of the principal avenues which connect the city centre with the outskirts – Corso Regio Parco and Corso Giulio Cesare –, the second historical city limit – created for toll payments in 1912 – and an abandoned railway trench, the core of the redevelopment of the district.

Four publicly owned reference buildings were selected to observe the variability both within the year and derived from the differences in the

Table 1
Cumulative number of the significant day and number of days for each month.

	January	February	March	April	May	June	July	August	September	October	November	December
Cumulative day number of the year	17	47	75	105	135	162	198	228	258	288	318	344
Number of days in the month	31	28	31	30	31	30	31	31	30	31	30	31

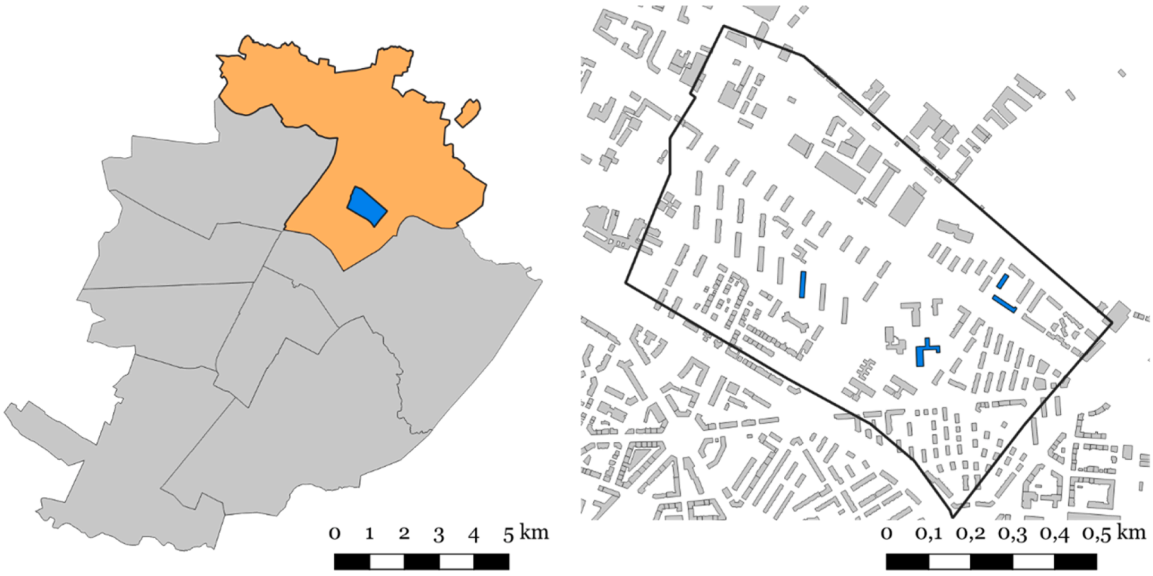

Fig. 2. Localisation of the area of interest (left) and of the representative buildings (right). District 6 is highlighted in orange within the City of Turin.

input values. It is necessary to have a heterogeneous sample – in terms of roof characteristics and orientation – to fully understand the variations derived from the high-resolution DSM and make the study representative of most building typologies in the city. The selected buildings – plotted in Fig. 3 – are:

- Building 1: two-pitched roof with dormers on one pitch and chimneys on the other, North-South orientation;
- Building 2: four-pitched roof with chimneys on one pitch, Northwest-Southeast orientation;
- Building 3: four-pitched roof with chimneys on the two larger pitches, Southwest-Northeast orientation;
- Building 4: complex roof, characterised by several pitches and affected by shadows from neighbouring elements – mostly trees.

The first two buildings are located along Via Pergolesi, while the other two are at the crossing between Corso Taranto and Via Ancina.

It is possible to refer to single buildings by resorting to the zonal statistics tool, which calculates the principal statistical indicators – as average, median, minimum, maximum, and standard deviation – for user-defined subsets provided as vector overlay layers.

3. Results

The principal findings of the research are reported first providing insights on the weather parameters gathered for the Area of Interest (A0I) – considering the principal trends throughout the year and comparing different data sources and aggregations – and then focusing on the outputs of the solar radiation estimation – performed with r.sun. insoltime tool in QGIS. Specific attention is devoted to monthly and seasonal trends, highlighting potential differences between buildings with different characteristics.

3.1. Data gathering

3.1.1. Digital Elevation Model

In the calculation of solar radiation, the principal input to estimate geographic and geometrical parameters is the Digital Elevation Model. Depending on the extension and characteristics of the area, it could be sufficient to use a Digital Terrain Model – returning the elevation of the bare earth without any extrusion – or preferably a Digital Surface Model (DSM), which represents the surface objects from the real world – both natural and anthropic – in addition to the exposed terrain. Given the complexity of the urban morphology and the need for accurate estimation of slope and orientation of the analysed pitches, for this study it was

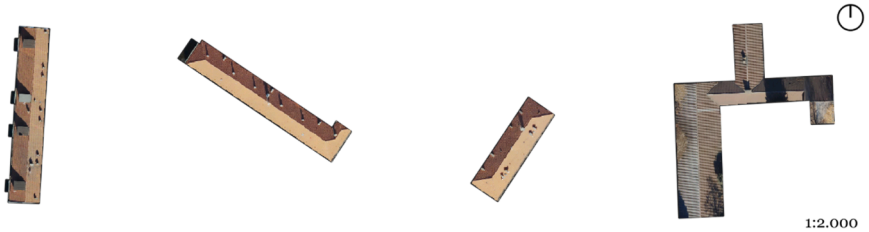

Fig. 3. Schematic representation of reference buildings' roofs.

necessary to use a high-resolution DSM.

On 29th January 2022 Compagnia Generale Ripreseaeree S.p.a. acquired photogrammetric pictures and LiDAR (Light Detection And Ranging) data on the whole City of Turin with a Leica CityMapper-2S Digital sensor. The acquisition was performed with a Piper PA31 plane at a calibrated altitude of approximately 1500 m. As a result, the density of the acquired LiDAR point cloud from which the DSM was produced turned out to be approximately 40 points/m^2.

The resulting DSM has a spatial resolution of 0.5 m. As shown in Fig. 4 – a sample of the DSM around building 4 – this gives the possibility of producing high-resolution elaborations, based on the clear identification of pitches and potentially disturbing elements, as chimneys and dormers. In particular, it is possible to see the complex structure of tree crowns, the different pitches and some chimneys on the neighbouring buildings.

3.1.2. Linke Turbidity Factor

Seven different values were considered for the Linke Turbidity Factor – four from Meteonorm (Meteotest, 2024) and the remaining from SoDa (Solar Energy Services for Professionals, 2022) and values included in a study by Fracastoro et al. (2011) and as r.sun default values (Hofierka et al., 2024).

With regard to the yearly aggregation, the highest value – 4.27 – derives from the research by Fracastoro et al. (2011), who performed acquisitions on the roof of the main campus of the Polytechnic University of Turin in 1975–1976 and 2010. On the other hand, aggregate values from Meteonorm ground measurements are the lowest – 3.01 and 3.24.

When refining the temporal resolution up to a four-month average, different trends emerge. In particular, while the values calculated by Fracastoro et al. are the highest in winter – 0.66 more than the SoDa factor – and summer – with the margin on SoDa values reduced to 0.05 –, in spring and autumn SoDa values are 0.26 higher. Another relevant variation can be observed in the interpolated values, with values comparable to the highest ones in spring/autumn and summer and much lower – 25 % - compared to the highest.

In general, it is possible to observe the highest values in summer – up to 4.53 –, from 28 % to 39 % higher than the winter values. Indeed, Turin is characterized by high humidity values in summer, resulting in recurring mist. This reduces the permeability of the atmosphere, with suspended vapour particles causing scattering phenomena. It can be assumed that summer mist has a higher impact on Linke Turbidity Value than winter smog, which has its peaks in winter – caused by heating systems. The only exception is represented by the values calculated by Fracastoro et al. (2011), with a 9 % difference between winter and summer.

When the temporal resolution is further refined to monthly values – plotted in Fig. 5 –, the reduced difference between winter and summer values in the study by Fracastoro et al. (2011) is made evident by the flattening of the curve.

Meteonorm values have a significant difference, with interpolated and ground measurements being recurringly the lowest, while Aeronet values show values comparable to the highest ones. However, the last has a sharp decrease between October and November, from 4.19 to 2.91 (31 % decrease), resulting in winter values close to the other Meteonorm ones.

According to most sources, the Linke Turbidity factor has an increase from January until the peak in June, before a considerable decrease in July and a stabilisation in August. The remaining months see a constant decrease towards the winter minimums. An exception is represented by the default r.sun values (Hofierka et al., 2024), with a distribution closer to the normal one: the peak is observed in July, with slight increases in the first part of the year, followed by a similar decrease in the second.

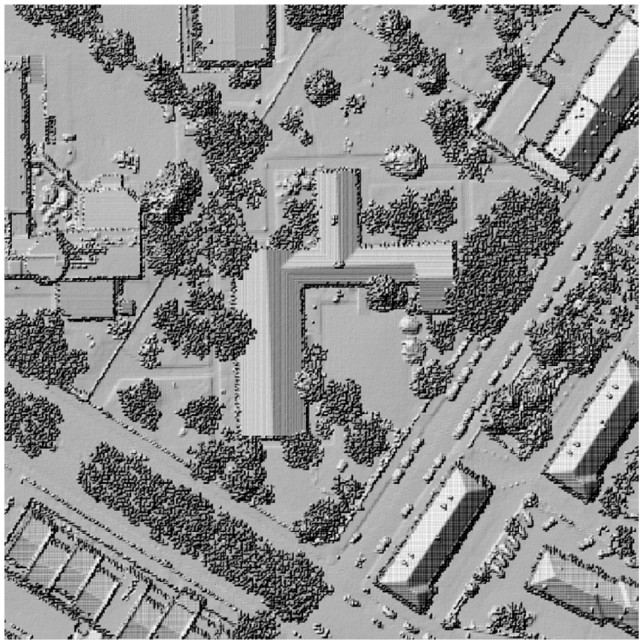

Fig. 4. Digital Surface Model.

3.1.3. Diffuse-to-Global radiation ratio

Four DG ratio values have been gathered: three derived from Meteonorm – Aeronet values are not available for this indicator – and one from PVGIS.

PVGIS values are nearly double compared to the Meteonorm ones, which are comparable. Indeed, the latter range from 18 % to 20 % on an annual scale, while the one calculated by the Joint Research Centre is 41 %. Contrary to the Linke Turbidity factor, the DG ratio has reduced differences among seasonal values. The deviation between seasonal values is 2 % for Meteonorm values, 4 % according to PVGIS.

When considering the highest temporal resolution considered – monthly – these variations are increased to 7 % for Meteonorm values and 13 % for PVGIS. Contrary to what happens for the Linke Turbidity Factor, maximum values are observed in winter – the maximum Meteonorm values of about 23 % occur in February – and autumn – according to PVGIS the share of scattered radiation in October is 48 %. A difference between the two sources emerges as Meteonorm locates its minimum – 16 % – in September, while July is the month where the share of diffuse radiation is less according to PVGIS. Fig. 6 shows the monthly variations of the DG ratio throughout the year. It can be observed that, compared to the Linke Turbidity Factor, there is a general flattening of the curve, without clear trends throughout the year but rather monthly fluctuations.

3.1.4. Test planning

Once having gathered the necessary parameters for r.sun.insoltime tool, these were included in a database to be used as the input for the solar radiation estimation.

According to the seven Linke Turbidity Factor and four DG ratio values, 28 possible yearly input combinations can be drafted. Each yearly combination is replicated once with yearly, once with seasonal and once with monthly input configurations. This resulted in 84 yearly elaborations and 1008 monthly values. All combinations are characterised with a univocal code: Y for yearly inputs, S for seasonal and M for monthly, followed by a progressive number from 01 to 28. Table 2 reports the progressive number of each combination.

Simulations are ordered first according to the DG ratio and then to the turbidity factor. For example, simulations from 01 to 08 use the DG ratio derived from ground-based Meteonorm measurements – the lowest –, and Turbidity factors from the lowest – Meteonorm weather stations – to the highest – gathered from Fracastoro et al. (2011).

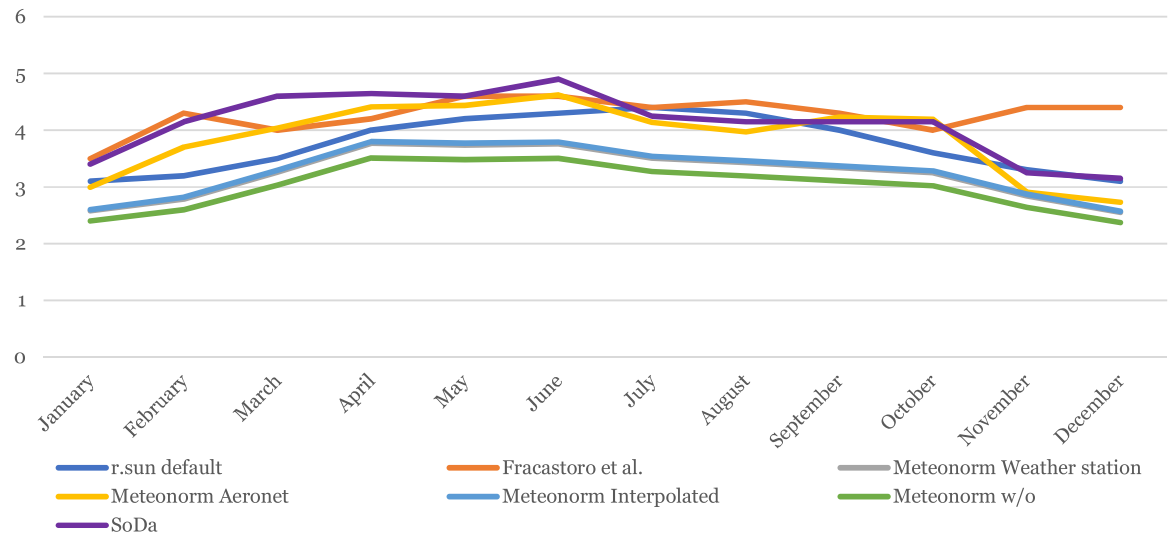

Fig. 5. Monthly values of Linke Turbidity Factor.

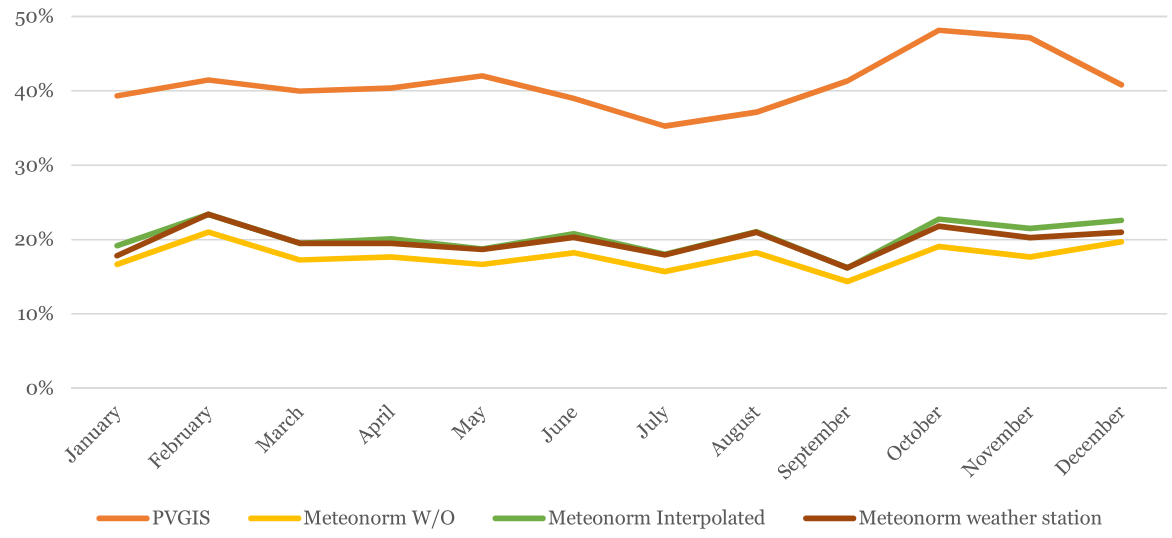

Fig. 6. Monthly values of Diffuse-to-Global radiation ratio.

Table 2
Progressive number of test plans with DG ratio and Linke Turbidity Factor specifications.

		DG Ratio			
		Meteonorm W/O	Meteonorm weather station	Meteonorm interpolated	PVGIS
Linke Turbidity Factor	Meteonorm W/O	01	08	15	22
	Meteonorm weather station	02	09	16	23
	Meteonorm interpolated	03	10	17	24
	r.sun default values	04	11	18	25
	Meteonorm Aeronet	05	12	19	26
	SoDa	06	13	20	27
	Fracastoro et al.	07	14	21	28

3.2. Solar radiation estimation

As mentioned in the methodology, three composite functions have been realised with the QGIS Graphical Modeller, one for each category of inputs: yearly, seasonal and monthly. Fig. 7 shows the graphical user interface of the yearly function, requiring the user to input the DSM, the two principal meteorological parameters and the vector file of the volumetric units to compute the aggregated values.

Once the user runs the composite function, the model produces the necessary inputs by running slope and orientation functions – calculating the results based on the DSM – and the "create constant raster" tool to realise the Linke turbidity factor and DG ratio raster files. For both weather parameters, the model creates a different number of files, based on the input aggregation level: one for the yearly values, three for the seasonal, and twelve for the monthly. Moreover, by subtracting the share of diffuse radiation to the global radiation, the share of beam radiation is returned too. The software automatically runs the solar radiation simulations for each month – based on the number of day of the

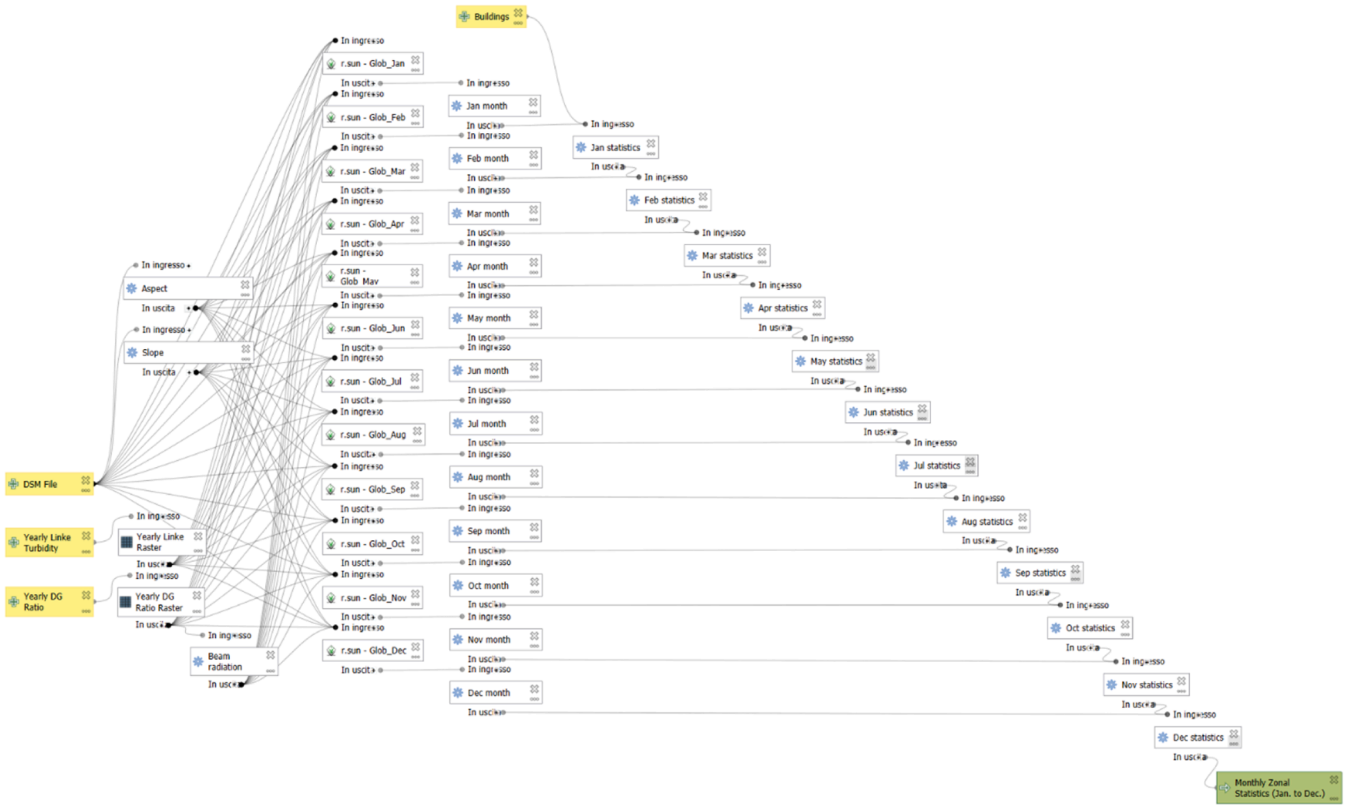

Fig. 7. Composite function for the solar radiation estimation with yearly input aggregation.

year set by default for each month – with r.sun.insoltime and multiplies the output to return the monthly radiation with the raster calculator. An example of the intermediate product of solar radiation maps is shown in Fig. 8. Finally, the zonal statistics tool refers all monthly radiation values to the user-defined volumetric units.

3.2.1. *Yearly results*

The analysis started from a coarse temporal resolution, considering yearly aggregates. This step is intended to extract the global trends and main differences among the trends, also paying specific attention to the differences between different input configurations (monthly, seasonal or yearly averages). Fig. 9 returns the median solar irradiation value over a year on building 4. Similar trends can be observed for the other buildings too.

Fig. 8. Solar radiation map, output of r.sun.insoltime.

The first observation derives from a clear difference that emerged within DG ratio values, with PVGIS showing the highest share of diffuse radiation – as explained in Section 3.1.3 Diffuse-to-Global radiation ratio. As a consequence, solar radiation estimations from the last groups (plans from 22 to 28) are generally lower compared to the others. Moreover, the DG ratio has a higher impact on solar radiation compared to the Linke turbidity factor. Indeed, differences within the group of PVGIS DG ratio are considerably flattened compared to the ones within the other groups. Nevertheless, there is always a difference, with radiation decreasing as the Linke and DG ratio values increase. As a result, solar radiation is maximum according to plan 01 – with Meteonorm ground observations for both DG ratio and Linke – and minimum according to plan 28 – PVGIS DG ratio and Fracastoro et al. Linke. For building 4, the difference is slightly higher than 0.2 MWh/m^2, equal to 31 %.

In addition to the differences between different calculation plans, there are reduced variations within each plan, deriving from the input aggregation. In general, there is a general tendency towards overestimation when computing solar radiation by inputting values aggregated on yearly values – the simplest model. This increase in values – on average 2 % for building 4 – has as the only exception the last plan, the one with the highest values of Linke turbidity factor – according to Fracastoro et al. (2011) – and DG ratio – obtained from PVGIS (European Commission, 2022c). In this case, the values are 0.5 % lower for building 4, but in all plans which consider the same Linke values it can be observed a reduced difference compared to other input configurations. On the other hand, there is a lighter discrepancy between values deriving from monthly and seasonal inputs. It is maximal for the plan of each DG ratio group which considers as Linke turbidity factor the default r.sun values (Hofierka et al., 2024).

Finally, the median values of all plans were computed to observe the differences between the different buildings, keeping the differentiation between input configurations – plotted in Fig. 10. First, it can be

Fig. 9. Median solar irradiation on building 4, differentiated by input level of aggregation.

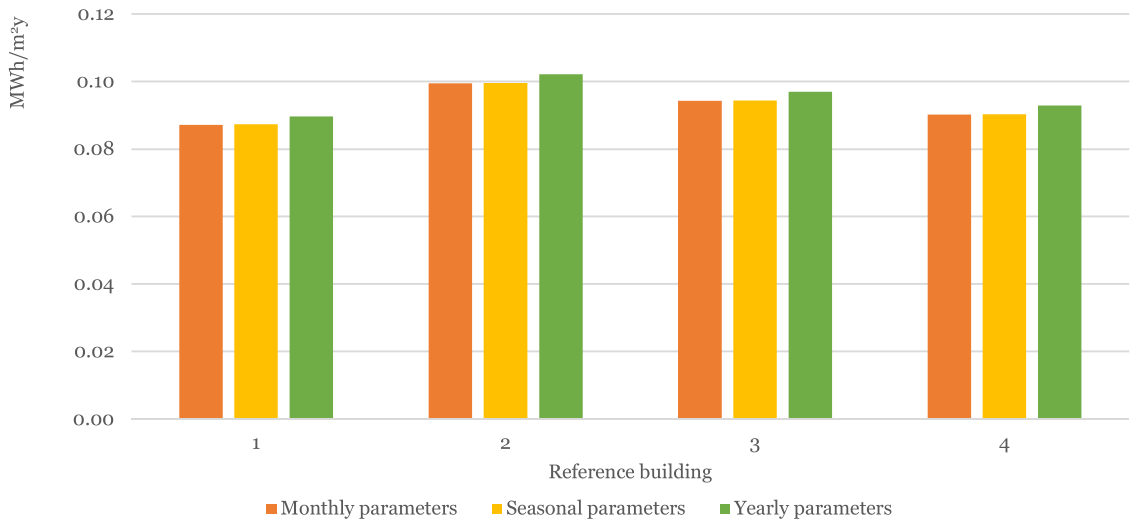

Fig. 10. Median yearly production values for the four reference buildings.

observed that a yearly input configuration leads to an overestimation in all four buildings – averaging a +2 % deviation compared to the monthly output. On the contrary, there is a reduced difference between the outcomes of the elaborations considering seasonal and monthly aggregations – +0.29 % on average, with a maximum discrepancy equal to 0.31 % in the case of building 3.

The most productive building is building 2, favoured by its orientation. Indeed, one of its pitches is oriented towards the southwest, maximising the afternoon solar radiation. On the contrary, building 1 has a lower productivity due to its North-South orientation, the most unfavourable. Intermediate conditions can be observed for buildings 3 and 4. The former takes advantage of morning radiation, while the latter is favoured by the complex geometry of its roof, making it possible to always have one pitch stroke by solar radiation.

In literature, several scholars have set a minimum annual solar radiation value as the threshold for assessing the suitability of an area to install PV panels. These thresholds vary from 700 kWh/m^2 according to Gawley and McKenzie (Gawley and McKenzie, 2022) to 1355 kWh/m^2 when considering the study by Hafeez and Atif (2015). Intermediate values are 925 kWh/m^2 (Pedrero et al., 2019), 1000 kWh/m^2 (Saadaoui et al., 2019) and 1100 kWh/m^2 (HosseiniHaghighi et al., 2022). However, these works consider case studies in countries characterised by high values of solar radiation – such as Morocco and Pakistan; therefore, the less restrictive value – 700 kWh/m^2 – can be adopted, leading to classify all the four considered buildings as suitable for PV production.

3.2.2. *Monthly trends*

After having observed the general differences within plans, it is possible to refine the temporal resolution and consider monthly variations of the solar radiation.

Based on the recognition of a difference between the annual results produced by the elaborations with different input aggregation, it is relevant to understand if these discrepancies could be observed throughout the whole year or are limited to specific months. To do so, Fig. 7 returns the elaborations for building 4 of test plans 01 and 28 with the three input configurations. These two test plans, using the maximum and minimum values – respectively – of both the Linke Turbidity Factor and DG ratio, are indicative of the principal trends. Figs. 11–13

On average, values returned by plan 01 are 26.1 % higher than the ones of plan 28. Differences between elaboration using yearly averages are 0.37 % higher compared to the ones with monthly inputs, with

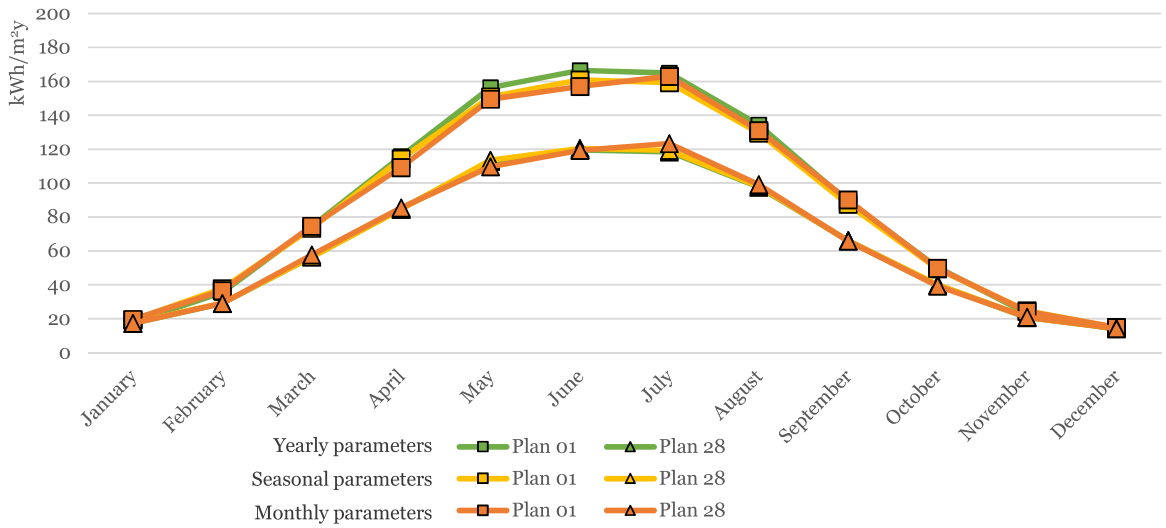

Fig. 11. Monthly solar radiation calculated according to plans 01 and 28.

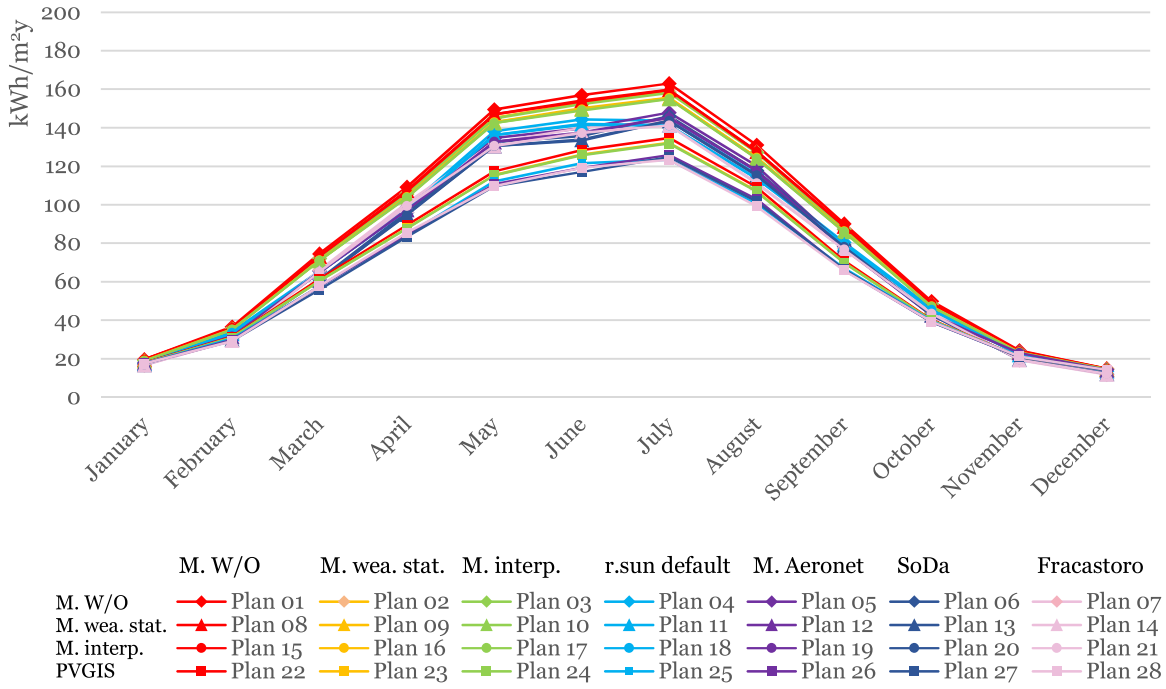

Fig. 12. Comparison of results from elaborations with monthly inputs.

seasonal averages returning intermediate values. The highest difference – 39.25 %, corresponding to 47 kWh/m^2 – can be observed in June between outputs considering yearly inputs, while the minimum is 311 kWh/m^2, or 2.17 % – in December considering seasonal inputs. In general, It can be observed that for all three input configurations differences are minimal – both in terms of percentage difference and absolute values – during winter, when solar radiation is lower, while considerable throughout spring, summer and autumn months. The second major difference which emerges is a shift in the peak production. While yearly and seasonal inputs reach their maximum in June, when calculating using monthly inputs an increase in solar radiation can be observed from May to July, with lower values in June (-5.7 % compared to yearly inputs).

The same trends can be observed when considering the differences within the same plan. In particular, focusing on plan 01, during winter the yearly and seasonal inputs lead to a general underestimation of solar radiation, while summer months are characterised by the opposite tendency. Nevertheless, monthly differences never exceed ±9 %. This difference is not observable in plan 28, where values generally overlap. On average, differences between the outputs with yearly and monthly inputs are −0.7 % and 0.2 %, respectively, corresponding to less than 0.4 kWh/m^2.

Secondly, all 28 plans are compared, taking advantage of Fig. 8, which categorises results from monthly inputs based on both DG ratio – with the same colour – and Linke turbidity factor – with the same symbol.

In general, the differences in input parameters cause a shift of the curves, with decreasing Linke turbidity factor and DG ratio causing an increase in the calculated solar radiation. Still, the trends are similar, with the minimum in December and the maximum in June. After the year starts, there is a general decrease of radiation – −3.8 % on average – in February. On the contrary, March is characterised by the highest

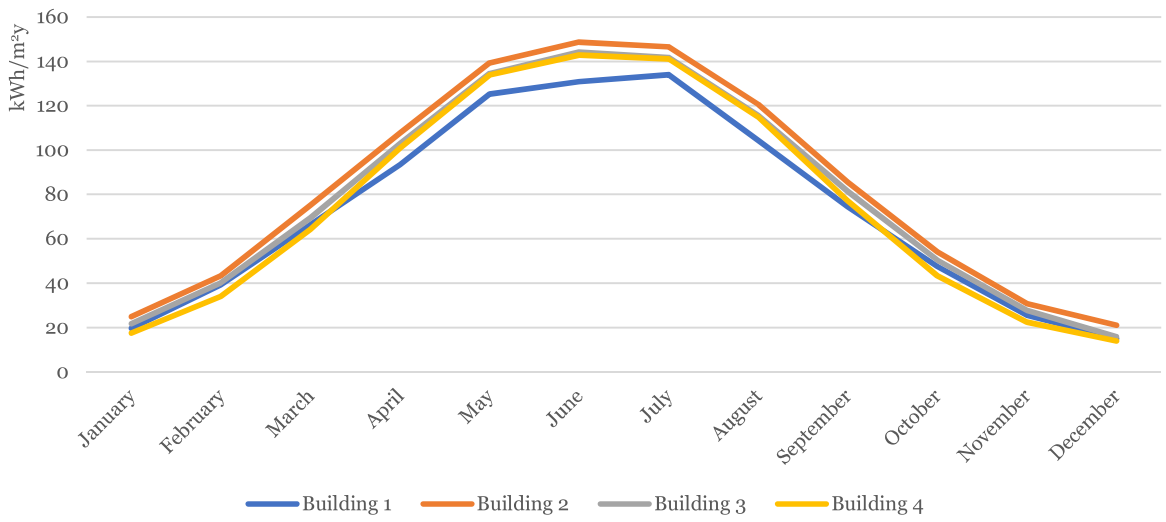

Fig. 13. Monthly median radiation for the four analysed buildings.

monthly variations – +26 % on average, with a maximum of +41 % in plan 14 (employing Meteonorm weather station DG ratio and Linke turbidity from Fracastoro et al.) –, followed by a light stabilisation in April. After another increase in May – +15 % – summer months are characterised by general stability, with all variations in the order of ±10 %. September has the highest negative difference – −16 % – and it is followed by further decreases of around 10 %. In absolute terms, variations are comprised between −18 kWh/m^2 and +39 kWh/m^2.

As for the yearly value, a final comparison considers the whole set of analysed buildings. Fig. 9 plots the median solar radiation for each building.

It is interesting to note that building 1 has a slight difference in the summer trends compared to the other three buildings, as it has its solar radiation maximum in July, while the others show a more consistent increase from May to June and a slight decrease in the following month. Building 4 has the widest differences between winter and summer, with the lowest values from January to March and from October to December and values comparable to the most productive buildings during summer. Throughout the whole year, building 2 shows the highest values, thus suggesting that a North-West South-East orientation is the most suitable.

4. Discussion

In the previous sections, only the median production values of each plan have been considered. However in order to obtain a variability range of the solar radiation estimation, it is relevant to note, for each roof, what are the trends of the minimum and maximum values, comparing them to the median. Fig. 14 returns minimum, median and maximum monthly values for building 4.

First, minimum values range from 2 kWh/m^2 to 6 kWh/m^2. These values, close to the null radiation, are mostly caused by the presence of disturbing elements, such as chimneys and dormers, casting shadows which limit the incident radiation to a small part of the diffused. On the contrary, maximum values in all months but December exceed 100 kWh/m^2 of solar radiation. Maximum values have high variability between summer and winter months – 88 % difference between July and December, corresponding to 80 kWh/m^2 – but a flattened distribution compared to median values – for which the percentage difference between the values of the same months is 957 %, equal to 130 kWh/m^2. Nevertheless, the value distribution is similar to the one of median values – with the highest increase in March, the most notable decrease in September and the peak in July. From this it emerges that both minimum and maximum values are flawed, thus making the calculation of the average solar radiation of the roof not accurate and not to be preferred over the median.

Once having chosen to compute the output variability range on the median, it is necessary to observe the differences between the 28 plans across the four buildings. Across the four reference buildings, the values of the plan returning the lowest and highest solar radiation are compared to the median in order to derive the output variability range. It emerged that there is a wider range between minimum and median value – (23 %) than between maximum and median (17 %). This

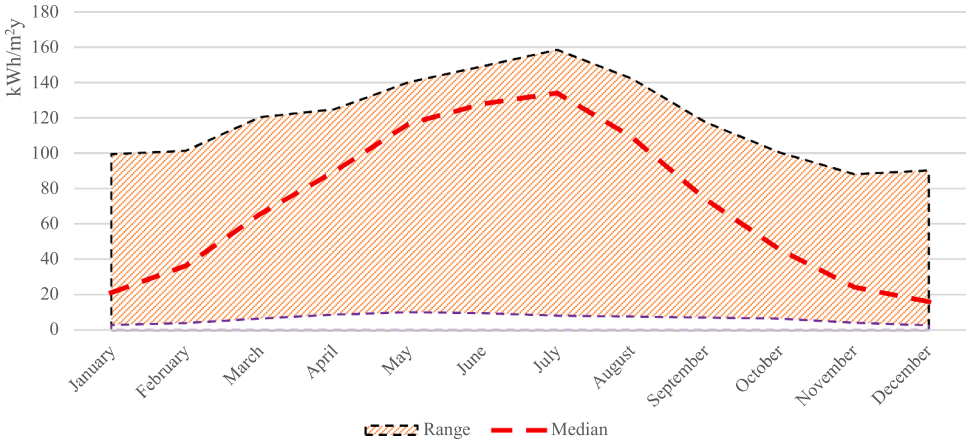

Fig. 14. Range between minimum and maximum values for each month compared to the median for building 4.

difference is quantified to be -30 kWh/m^2 and $+23$ kWh/m^2, respectively. These values are observed in the whole set of reference buildings, characterised – as mentioned – by heterogeneous characteristics, with variations from the explicated averages in the order of ± 1 %. Therefore, it can be concluded that the variability range is quantified to be around ± 20 %.

5. Conclusion and future developments

This research started from the recognition of both the key role photovoltaic technologies have in the context of energy transition, thanks to the limited land take and the possibility to produce energy where it is needed – relevant for energy communities –, and the need for tools supporting their efficient installation. As Geographic Information Systems have been used for computing solar radiation – the most complex parameter to be modelled – in multiple studies worldwide without assessing their precision or accuracy, the main goal of the study has been to define an output variability range for GIS-based solar radiation estimations.

The whole process has been carried out in QGIS software, resorting to the r.sun.insoltime tool – originally developed in GRASS GIS and now integrated into QGIS – for the computation of solar radiation. The first part of the study was about understanding the necessary data to be used as inputs and gathering them. In particular, three sources (PVGIS, Meteonorm and SoDa) were used for monthly values of Linke turbidity factor and share of diffuse to global radiation. Once having obtained data, these were crossed in all possible combinations to create 28 typical years and for every year yearly and seasonal aggregates were computed. Solar radiation was calculated for all 28 typical years with the three input configurations (monthly, seasonal and yearly) and compared on four reference buildings – heterogeneous in terms of roof characteristics and orientation.

According to the findings of this study – described in the previous two sections – it is possible to draw some conclusions and define the main elements to be considered when continuing the research.

The first major finding is the optimal input configuration selection, which resulted to be the seasonal. Indeed, it simplifies the model – requiring ¼ of the parameters required when considering monthly inputs – but keeps a good precision compared to the latter, with an overestimation averaging 0.2 %. Yearly input configurations lead to a general overestimation of the results, making it necessary to define site-specific correction factors to post-process the solar radiation estimation. While site-specificity is considered to be an added value for this research – thanks to the possibility of providing an extensive analysis of a single case study with homogeneous characteristics rather than generalising the outputs of heterogeneous areas – it also represents a limitation. Indeed, these results cannot be generalised, as they are valid for the City of Turin and areas with similar weather conditions. Nevertheless, it is possible to apply the same methodology to define the output variability range elsewhere, thus contributing to the creation of a large dataset with multiple localities. Moreover, some findings can be generalised, too. For instance, it is likely to observe everywhere the widest differences in summer months, where solar radiation is maximum, as similar percentage differences lead to higher absolute differences when numerical values are higher.

As initially stated, the main goal of this research was to define a variability range which quantifies the precision of solar radiation estimations when considering alternative input sources. Based on a high variability in the inputs – in particular, the share between diffuse and global radiation has a 100 % discrepancy between alternative sources – relevant differences could be observed among the 28 test plans carried out in this research, combining the different inputs. As a result, the output variability range was quantified to be ± 20 % monthly. This results in the possibility to perform accurate analyses, predicting the incoming solar radiation for photovoltaic system installation.

Nevertheless, it is possible to define some elements to be considered for further refining this study. First, some energy-related aspects can be considered. At this step the focus was put on simulation precision, while simulation accuracy with respect to reality was not tackled. A reliable validation dataset would be necessary to assess if the so-optimized simulation methodology quantifies the solar potential effectively. Validation could be performed in a twofold way, either by acquiring a historical series from existing systems and databases or using real-world data from weather stations or photovoltaic panels – to be acquired for the research. Moreover, the correlation – the temporal shift between the peaks in production and consumption, resulting in the need for storing energy – has to be considered, on a seasonal and daily basis. Once having identified the most suitable buildings for the installation of solar technologies, refining the temporal resolution of the analysis is crucial in order to define the size of the required system. Moreover, urban contexts are complex by definition, with different geometries and materials. As a result, reflections of solar radiation can occur. Albedo is the principal indicator used to quantify reflectance: when considered, it results in an increase in global solar radiation striking urban surfaces. In this research it was not considered because of the generally low resolution at which it is computed – in many studies it is estimated from satellite measurements –, likely to cause recurring biases. Moreover, the area of interest is characterised by the use of little reflecting materials, such as roof tiles and plastered walls, rather than specular and glazed surfaces. Nevertheless, in the case of the possibility to have the availability of accurate albedo estimation, it is possible to consider this parameter in the solar radiation calculation, further refining the outcome accuracy.

The two final concluding remarks concern geometric factors. First, similarly to what was done for the level of aggregation of inputs, the differences emerge when considering coarser Digital Surface Models, with ground sampling distances of 1 m or 5 m – generally available open source – compared to the one of 0.5 m employed in this research. Furthermore, it is possible to consider not only buildings as a whole but also extract the pitches. Indeed, it was observed in paragraph 3.1.1. Digital Elevation Model that it is likely that some pitches – facing Southwards – guarantee higher production compared to others – typically the ones oriented to the North. The extraction of pitches from LiDAR point clouds or the DSM could represent a significant step towards the realisation of an efficient tool for supporting the planning of solar technology installations.

Acronyms

AoI	Area of Interest
ASR	Area Solar Radiation
DG ratio	Diffuse-to-Global radiation ratio
DSM	Digital Surface Model
GIS	Geographic Information System
PV	Photovoltaic
PVGIS	Photovoltaic Geographical Information System
RES	Renewable Energy Source

CRediT authorship contribution statement

Sebastiano Anselmo: Writing – original draft, Visualization, Validation, Methodology, Formal analysis, Data curation. **Ali Safaeianpour:** Visualization, Software, Investigation. **Sara Torabi Moghadam:** Supervision, Methodology, Conceptualization. **Maria Ferrara:** Writing – review & editing, Supervision, Methodology, Conceptualization.

Declaration of Competing Interest

The authors declare that they have no known competing financial interests or personal relationships that could have appeared to influence the work reported in this paper.

Data Availability

Data will be made available on request.

References

Agugiaro, G., Remondino, F., Stevanato, G., De Filippi, R., Furlanello, C., 2013. Estimation of solar radiation on building roofs in mountainous areas. Int. Arch. Photogramm., Remote Sens. Spat. Inf. Sci. 38, 155–160. https://doi.org/10.5194/isprsarchives-XXXVIII-3-W22-155-2011.

Anselmo, S., Ferrara, M., 2023. Trends and Evolution of the GIS-Based Photovoltaic Potential Calculation. Energ. (Basel) 16, 7760. https://doi.org/10.3390/en16237760.

Anselmo, S., Ferrara, M., Corgnati, S.P., Boccardo, P., 2023. Aerial urban observation to enhance energy assessment and planning towards climate-neutrality: A pilot application to the city of Turin. Sustain Cities Soc. 99. https://doi.org/10.1016/j.scs.2023.104938.

Bódis, K., Kougias, I., Jäger-Waldau, A., Taylor, N., Szabó, S., 2019. A high-resolution geospatial assessment of the rooftop solar photovoltaic potential in the European Union. Renew. Sustain. Energy Rev. 114, 109309. https://doi.org/10.1016/j.rser.2019.109309.

Bremer, M., Mayr, A., Wichmann, V., Schmidtner, K., Rutzinger, M., 2016. A new multi-scale 3D-GIS-approach for the assessment and dissemination of solar income of digital city models. Comput. Environ. Urban Syst. 57, 144–154. https://doi.org/10.1016/j.compenvurbsys.2016.02.007.

Coakley, J.A., 2003. Reflectance and Albedo, Surface. in: Encyclopedia of Atmospheric Sciences. Elsevier, pp. 1914–1923. https://doi.org/10.1016/B0-12-227090-8/00069-5.

Desthieux, G., Carneiro, C., Camponovo, R., Ineichen, P., Morello, E., Boulmier, A., Abdennadher, N., Dervey, S., Ellert, C., 2018. Solar Energy Potential Assessment on Rooftops and Facades in Large Built Environments Based on LiDAR Data, Image Processing, and Cloud Computing. Methodological Background, Application, and Validation in Geneva (Solar Cadaster). Front Built Environ. 4. https://doi.org/10.3389/fbuil.2018.00014.

Eldesoky, A.H., Colaninno, N., Morello, E., 2019. An integrated, agile approach for estimating solar radiation on building facades in complex urban environments. : J. Phys.: Conf. Ser. https://doi.org/10.1088/1742-6596/1343/1/012015.

Eltbaakh, Y.A., Ruslan, M.H., Alghoul, M.A., Othman, M.Y., Sopian, K., Razykov, T.M., 2012. Solar attenuation by aerosols: An overview. Renew. Sustain. Energy Rev. 16, 4264–4276. https://doi.org/10.1016/j.rser.2012.03.053.

Esclapés, J., Ferreiro, I., Piera, J., Teller, J., 2014. A method to evaluate the adaptability of photovoltaic energy on urban façades. Sol. Energy 105, 414–427. https://doi.org/10.1016/j.solener.2014.03.012.

European Commission, 2023. EU Mission: Climate-Neutral and Smart Cities [WWW Document]. URL https://research-and-innovation.ec.europa.eu/funding/funding-opportunities/funding-programmes-and-open-calls/horizon-europe/eu-missions-horizon-europe/climate-neutral-and-smart-cities_en#documents (accessed 3.2.24).

European Commission, 2022a. Communication from the Commission to the European Parliament, the Council, the European Economic and Social Committee and the Committee of the Regions. REPowerEU Plan.

European Commission, 2022b. Communication from the Commission to the European Parliament, the Council, the European Economic and Social Committee and the Committee of the Regions. EU Solar Energy Strategy.

European Commission, 2022c. PVGIS 5.2 [WWW Document]. URL https://joint-research-centre.ec.europa.eu/photovoltaic-geographical-information-system-pvgis/pvgis-releases/pvgis-52_en (accessed 2.2.24).

European Parliament and Council, 2009. Directive 2009/28/EC of the European and of the Council of 23 April 2009 on the promotion of the use of energy from renewable sources and amending and subsequently repealing Directives 2001/77/EC and 2003/30/EC.

European Parliament and Council, 2018. Directive (EU) 2018/2001 of the European Parliament and of the Council of 11 December 2018 on the promotion of the use of energy from renewable sources (recast).

European Parliament and Council, 2024. Directive (EU) 2024/1275 of the European Parliament and of the Council of 24 April 2024 on the energy performance of buildings (recast).

Fichera, A., Gagliano, A., Nocera, F., Pagano, A., Volpe, R., Bisegna, F., 2018. Application of a Geographical Information System to Plan Energy Policy at a Neighborhood Scale, in: Proceedings - 2018 IEEE International Conference on Environment and Electrical Engineering and 2018 IEEE Industrial and Commercial Power Systems Europe, EEEIC/I and CPS Europe 2018. https://doi.org/10.1109/EEEIC.2018.8493723.

Fijałkowska, A., Waksmundzka, K., Chmiel, J., 2022. Assessment of the Effectiveness of Photovoltaic Panels at Public Transport Stops: 3D Spatial Analysis as a Tool to Strengthen Decision Making. Energ. (Basel) 15. https://doi.org/10.3390/en15031230.

Fracastoro, G.V., Yang, Y., Simonetti, M., Coppa, G., 2011. Atmospheric Turbidity Measurements in Torino: A Comparison Between 1975 and 2010 Data. in: Proceedings of the ISES Solar World Congress 2011. International Solar Energy Society, Freiburg, Germany, pp. 1–9. https://doi.org/10.18086/swc.2011.24.11.

Freitas, S., Catita, C., Redweik, P., Brito, M.C., 2015. Modelling solar potential in the urban environment: State-of-the-art review. Renew. Sustain. Energy Rev. 41, 915–931. https://doi.org/10.1016/j.rser.2014.08.060.

Gawley, D., McKenzie, P., 2022. Investigating the suitability of GIS and remotely-sensed datasets for photovoltaic modelling on building rooftops. Energy Build. 265. https://doi.org/10.1016/j.enbuild.2022.112083.

Hofierka, J., Suri, M., 2002. The solar radiation model for Open source GIS: implementation and applications., in: International GRASS Users Conference. Trento, Italy.

Hofierka, J., Suri, M., Huld, T., 2024. r.sun - GRASS GIS manual [WWW Document]. URL https://grass.osgeo.org/grass83/manuals/r.sun.html (accessed 11.1.23).

HosseiniHaghighi, S., de Uribarri, P.M.Á., Padsala, R., Eicker, U., 2022. Characterizing and structuring urban GIS data for housing stock energy modelling and retrofitting. Energy Build. 256. https://doi.org/10.1016/j.enbuild.2021.111706.

Hubinský, T., Hajtmanek, R., Šeligová, A., Legény, J., Špaček, R., 2023. Potentials and Limits of Photovoltaic Systems Integration in Historic Urban Structures: The Case Study of Monument Reserve in Bratislava, Slovakia. Sustain. (Switz.) 15. https://doi.org/10.3390/su15032299.

IEA, 2016. Energy Technologies Perspectives 2016. Available online: https://www.iea.org/reports/energy-technology-perspectives-2016. Paris.

Klein, S.A., 1977. Calculation of monthly average insolation on tilted surfaces. Sol. Energy 19, 325–329. https://doi.org/10.1016/0038-092X(77)90001-9.

Liang, J., Gong, J., 2017. A sparse voxel octree-based framework for computing solar radiation using 3d city models. ISPRS Int J. Geoinf. 6. https://doi.org/10.3390/ijgi6040106.

Liang, J., Gong, J., Li, W., Ibrahim, A.N., 2014. A visualization-oriented 3D method for efficient computation of urban solar radiation based on 3D-2D surface mapping. Int. J. Geogr. Inf. Sci. 28, 780–798. https://doi.org/10.1080/13658816.2014.880168.

Liang, J., Gong, J., Xie, X., Sun, J., 2020. Solar3D: An open-source tool for estimating solar radiation in urban environments. ISPRS Int J. Geoinf. 9. https://doi.org/10.3390/ijgi9090524.

Lindberg, F., Jonsson, P., Honjo, T., Wästberg, D., 2015. Solar energy on building envelopes - 3D modelling in a 2D environment. Sol. Energy 115, 369–378. https://doi.org/10.1016/j.solener.2015.03.001.

Lohani, B., Kumar Singh, S., Choudhary, D., Nagarajan, B., 2018. A new approach to determine solar potential using terrestrial images. Remote Sens. Lett. 9, 636–645. https://doi.org/10.1080/2150704X.2018.1452061.

Meteotest, 2024. Meteonorm [WWW Document]. URL https://meteonorm.com/en/ (accessed 5.28.24).

Minerva, R., Lee, G.M., Crespi, N., 2020. Digital Twin in the IoT Context: A Survey on Technical Features, Scenarios, and Architectural Models. Proc. IEEE 108, 1785–1824. https://doi.org/10.1109/JPROC.2020.2998530.

Mutani, G., Casalengo, M., Ramassotto, M.A., 2019. The effect of roof-integrated solar technologies on the energy performance of public buildings: the case study of the City of Turin (IT), in: INTELEC. Int. Telecommun. Energy Conf. (Proc.). https://doi.org/10.1109/INTLEC.2018.8612398.

Nakhaee, A., Paydar, A., 2023. DeepRadiation: An intelligent augmented reality platform for predicting urban energy performance just through 360 panoramic streetscape images utilizing various deep learning models. Build. Simul. 16, 499–510. https://doi.org/10.1007/s12273-022-0953-5.

Page, J.K., 1981. Radiation Data. in: Solar Energy Conversion II. Elsevier, pp. 23–35. https://doi.org/10.1016/B978-0-08-025388-6.50013-1.

Pedrero, J., Hermoso, N., Hernández, P., Munoz, I., Arrizabalaga, E., Mabe, L., Prieto, I., Izkara, J.L., 2019. Assessment of urban-scale potential for solar PV generation and consumption. : IOP Conf. Ser.: Earth Environ. Sci. https://doi.org/10.1088/1755-1315/323/1/012066.

Peng, F., Wong, M.S., Nichol, J.E., Chan, P.W., 2016. Historical GIS data and changes in urban morphological parameters for the analysis of urban heat islands in Hong Kong. : Int. Arch. Photogramm., Remote Sens. Spat. Inf. Sci. - ISPRS Arch. 55–62. https://doi.org/10.5194/isprsarchives-XLI-B2-55-2016.

Redweik, P.M., Catita, C., Brito, M.C., 2012. 3D Local Scale Solar Radiation Model Based on Urban LiDAR Data. Int. Arch. Photogramm., Remote Sens. Spat. Inf. Sci. 38 265–269. https://doi.org/10.5194/isprsarchives-XXXVIII-4-W19-265-2011.

Politecnico di Torino, 2024. SDG11 Lab [WWW Document]. URL https://sdg11.polito.it/en/node/37 (accessed 5.15.24).

Regione Piemonte, 2024. GeoPiemonte [WWW Document]. URL www.geoportale.piemonte.it (accessed 5.20.24).

Remund, J., Wald, L., Levèvre, M., Ranchin, T., Page, J.H., 2003. Worldwide Linke turbidity information, in: ISES Solar World Congress 2003. Goteborg, Sweden.

Remund, J., Müller, S., Schmutz, M., Barsotti, D., Graf, P., Cattin, R., 2023. Handbook part I: Software, in: Meteonorm 8. Irradiation Data for Every Place on Earth. Meteotest AG, Bern, pp. 1–81.

Ren, H., Ma, Z., Ming Lun Fong, A., Sun, Y., 2022. Optimal deployment of distributed rooftop photovoltaic systems and batteries for achieving net-zero energy of electric bus transportation in high-density cities. Appl. Energy 319. https://doi.org/10.1016/j.apenergy.2022.119274.

Saadaoui, H., Ghennioui, A., Ikken, B., Rhinane, H., Maanan, M., 2019. Using GIS and photogrammetry for assessing solar photovoltaic potential on Flat Roofs in urban area case of the city of Ben Guerir / Morocco. : Int. Arch. Photogramm., Remote Sens. Spat. Inf. Sci. - ISPRS Arch. 155–166. https://doi.org/10.5194/isprs-archives-XLII-4-W12-155-2019.

Singh, S.K., Lohani, B., Arora, L., Choudhary, D., Nagarajan, B., 2020. A visual-inertial system to determine accurate solar insolation and optimal PV panel orientation at a point and over an area. Renew. Energy 154, 223–238. https://doi.org/10.1016/j.renene.2020.02.107.

Soares, P., Bayrakci-Boz, M., Brownson, J.R.S., 2020. GIS Information for Solar PV Energy Siting: A Case Study in the Borough of State College, PA, USA, in: Conference Record of. IEEE Photovolt. Spec. Conf. 1749–1753. https://doi.org/10.1109/PVSC45281.2020.9300797.

Solar Energy Services for Professionals, 2022. SoDa [WWW Document]. URL https://www.soda-pro.com/ (accessed 2.15.24).
United Nations General Assembly, 2015. Resolution adopted by the General Assembly on 25 September 2015.
Yoon, D.H., Song, J.H., Koh, J.H., 2020. Estimation of solar radiation potential in the urban buildings using CIE Sky model and ray-tracing. Journal of the Korean Society of Surveying, Geodesy. Photogramm. Cartogr. 38, 141–151. https://doi.org/10.7848/ksgpc.2020.38.2.141.
Yu, H., Wang, M., Lin, X., Guo, H., Liu, H., Zhao, Y., Wang, H., Li, C., Jing, R., 2021. Prioritizing urban planning factors on community energy performance based on GIS-informed building energy modeling. Energy Build. 249, 111191. https://doi.org/10.1016/j.enbuild.2021.111191.